Chin. Sci. Bull. (2014) 59(33):4498–4509
DOI 10.1007/s11434-014-0367-6

csb.scichina.com
www.springer.com/scp

Article

Oceanology

Variations of alkenone temperature in the Sea of Japan during the last 170 ka and its paleoceanographic implications

Yanguang Liu · Jiaojie Chen · Jinxia Chen · Lei Xing · Jianjun Zou · Zhengquan Yao

Received: 14 January 2014 / Accepted: 14 March 2014 / Published online: 23 April 2014

Abstract Two sediment cores, KCES1 and ODP797, which were recovered from the Sea of Japan (JS), were measured for alkenone-derived sea surface temperatures ($U^{K'}_{37}$-SSTs). Our results revealed that the SSTs closely follow the glacial-interglacial cycles during the last 170 ka, except in the last glacial maximum (LGM), during which the SST was higher than in the Holocene. The anomalous high temperature in the LGM is considered as an effect of the intrusion of a low salinity water mass into the JS when the sea level was almost below 130 m. On the glacial-interglacial to orbital timescale, the $U^{K'}_{37}$-SSTs record in the JS correlated well with the benthic foraminiferal $\delta^{18}O$ record and solar insolation, which suggests the dominant control of solar insolation and its related sea ice development on the SST in the JS. On the sub-orbital/millennial timescale, reduced SST corresponds to an enhanced east asian winter monsoon (EAWM) during the last glacial period (MIS3 and MIS4), indicating the dominant control of sea ice expansion due to the enhanced EAWM on the SST in the JS. In contrast, during the last interglacial period (MIS5), the SST in the JS was controlled by variations in the east Asian summer monsoon. These results highlight the key role of solar insolation and associated glacial-interglacial conditions in the variations of the SST in the JS since the last 170 ka.

Keywords Sea of Japan · Alkenone · Paleotemperature · Last interglacial · East Asian Monsoon

1 Introduction

As one of the marginal seas of the northwestern Pacific, which was produced by the collision between the Euro-Asian and Pacific Ocean plates, the Sea of Japan (JS, called the East Sea in Korea) is considered an ideal place for the preservation of important paleoclimatic information. The JS was strongly influenced by the global sea level and East Asian Monsoon (EAM) system. During high sea level, the exchange of water mass between the JS and the surrounding sea areas occurs via the Tsushima Warm Current (TWC), which flows into the JS through the Korea-Tsushima Strait (KTS) and outflows through the Tsugaru and Soya Straits [1]. As the main source of energy and salinity of JS, the TWC influences the temperature and circulation of the JS [2, 3] as well as the atmospheric environments of JS and the adjacent land area [4]. In low sea level periods, most of the TWC warm and saline water mass was blocked due to the shallow straits [5]; therefore, the JS presented an independent and closed deposit environment. Hence, the JS surface temperatures (SSTs) were strongly affected by the fluctuation of the global sea level. In addition, the fluctuations of SSTs are also closely related with the seasonal changes in winds. During the winter monsoon season, a cold and dry northwesterly wind blows over the sea and induces a decrease of the SSTs and an increase of sea ice in the JS [6]. During the summer monsoon season, a warm

Y. Liu (✉) · J. Chen · J. Chen · J. Zou · Z. Yao
Key Laboratory of Marine Sedimentology and Environmental Geology, First Institute of Oceanography, State Oceanic Administration, Qingdao 266061, China
e-mail: yanguangliu@fio.org.cn

L. Xing
Key Laboratory of Marine Chemistry Theory and Technology, Ministry of Education/Qingdao Collaborative Innovation Center of Marine Science and Technology, Ocean University of China, Qingdao 266100, China

and humid southwest wind blows over it because of the enhanced North Pacific high-pressure system. This makes the area warmer than areas at the same latitude in Europe [7].

During the glacial/interglacial cycles, the sea level fluctuated between low/high stands, and the regional EAM varied between strong/weak; these fluctuations would be decipherable from the paleoceanographic archives, in particular, the SST records of the JS. Establishing the paleotemperature recorded in the JS is necessary for understanding the paleoceanographic changes in the sea and its response to global climate change.

Long-chain alkenones are generally produced by a special haptophyte microalgae under the open marine environment [8]. They are biolipids consisting mainly of C_{37}–C_{39} homologues with di-, tri-, and tetra- unsaturation in which the C_{37} alkenones include di-($C_{37:2}$), tri-($C_{37:3}$), and tetra-unsaturated ($C_{37:4}$) members. The unsaturation index of C_{37} alkenones, which are calculated using U^{K}_{37} $[(C_{37:2}+C_{37:4})/(C_{37:2}+C_{37:3}+C_{37:4})]$ or $U^{K'}_{37}$ $[C_{37:2}/(C_{37:2}+C_{37:3})]$, have a linear relationship with the sea surface water temperature where the algae has grown [9, 10]. The two most abundant species that produce alkenones are *Emiliania huxleyi* and *Gephyrocapsa oceanica*, which are ubiquitous in the ocean. Therefore, the relative ratios of $C_{37:3}$ and $C_{37:2}$ alkenones are well preserved in the marine sediments in spite of biodegradation [11–13]. As a useful paleothermometer, U^{K}_{37} and $U^{K'}_{37}$ have been applied worldwide in order to assess the SST by using gas chromatography measurements for marine sediments [7, 14–18].

Numerous studies of the SST-based paleoenvironmental evolution in the JS have been published since the 1990s [4, 7, 18–20]. Although many of these studies focused on the SST variations at different locations in the JS, long time-scale oceanographic variations of this area remain poorly understood. The regional climate influences, such as that of EAM on the JS, are rarely discussed, and therefore, the possible teleconnections between the JS and the global climate variations is not clear thus far. This paper presents the long-term $U^{K'}_{37}$-SSTs data to study the oceanographic changes of the JS in the glacial/interglacial cycles and its response to global climate change. Furthermore, the linkages between the water exchanges and the intensity of the regional EAM under the background of the eustatic sea level changes are discussed.

2 General setting and background

The JS is a semi-enclosed marginal sea bounded by the Japanese arc to the east, and the Korean peninsula and far-eastern Russia to the west. The sea is connected to the East China Sea, the Okhotsk Sea, and the northwest Pacific Ocean by six shallow and narrow straits with sill depths less than 140 m (Fig. 1a). The deep part of the JS is subdivided into three deep basins (Japan, Yamato, and Ulleung basins) that are separated by the topographic highs of the Korea Plateau, the Oki ridge, and the Yamato Rise. On the eastern shores, the continental shelves of the JS are relatively wide; however, shelves on the western shelves are narrow (Fig. 1b).

A distinct front (Sub-polar Front, SPF) exists at around 40°N, with a temperature gradient in the upper and intermediate waters (<400 m) of about 7 °C, with an annual mean ranging from about 5 °C in the north to about 12 °C in the south [1]. The deep and bottom water masses are distributed below 400 m and regulated by the Japan Sea Proper Water (JSPW), which is a relatively homogeneous water mass and characterized by low temperature (<1 °C), high salinity (about 34 ‰), and a high content of dissolved oxygen (5–6 mL/L) [21]. The well-ventilated JSPW is formed via winter convection that is enhanced by the salt import of the TWC, with the instabilities in the SPF serving to transport this salt into the northern deep-water formation regions [1, 22]. Driven by the winter monsoon, the cold and oxygen-rich surface water in the northwestern JS sinks and ventilates the bottom water, thereby increasing the oxygen level of the bottom water [23]. A radiocarbon-based study of seawater resulted in an estimated deep-water mass turnover rate in the JS of 100–300 years [24]. According to oceanographic studies, the TWC seasonally originates from the Taiwan Warm Current and the Kuroshio [25]. The temperature and salinity of TWC were influenced by fresh water discharges from the adjacent land and change seasonally (low temperature and high salinity in winter, high temperature and low salinity in summer) [5].

In response to the global sea level change, the paleoceanographic conditions of the JS fluctuated remarkably due to the dramatic variations in the influx of the East China Sea Coastal Water (ECSCW, partly influenced by the Changjiang Diluted Water (CJDW)) and the TWC via the shallow sill during the glacial periods (Fig. 1b). This variability in the exchange with the open ocean resulted in sedimentation under redox conditions of bottom water. The hemipelagic sediments of the JS are characterized by centimeter- to decimeter-scale alternations of organic-poor light-gray layers and organic-rich dark-gray layers [26]. The dark layers are mostly laminated, whereas, the light layers are homogeneous, bioturbated, and generally separated from the dark layers by sharp boundaries. These dark-light cycles are considered to be forming under frequent fluctuation between anoxic and/or oxic bottom water conditions basin-wide with millennial scale periodicity that are possibly associated with the Dansgaard-Oeschger

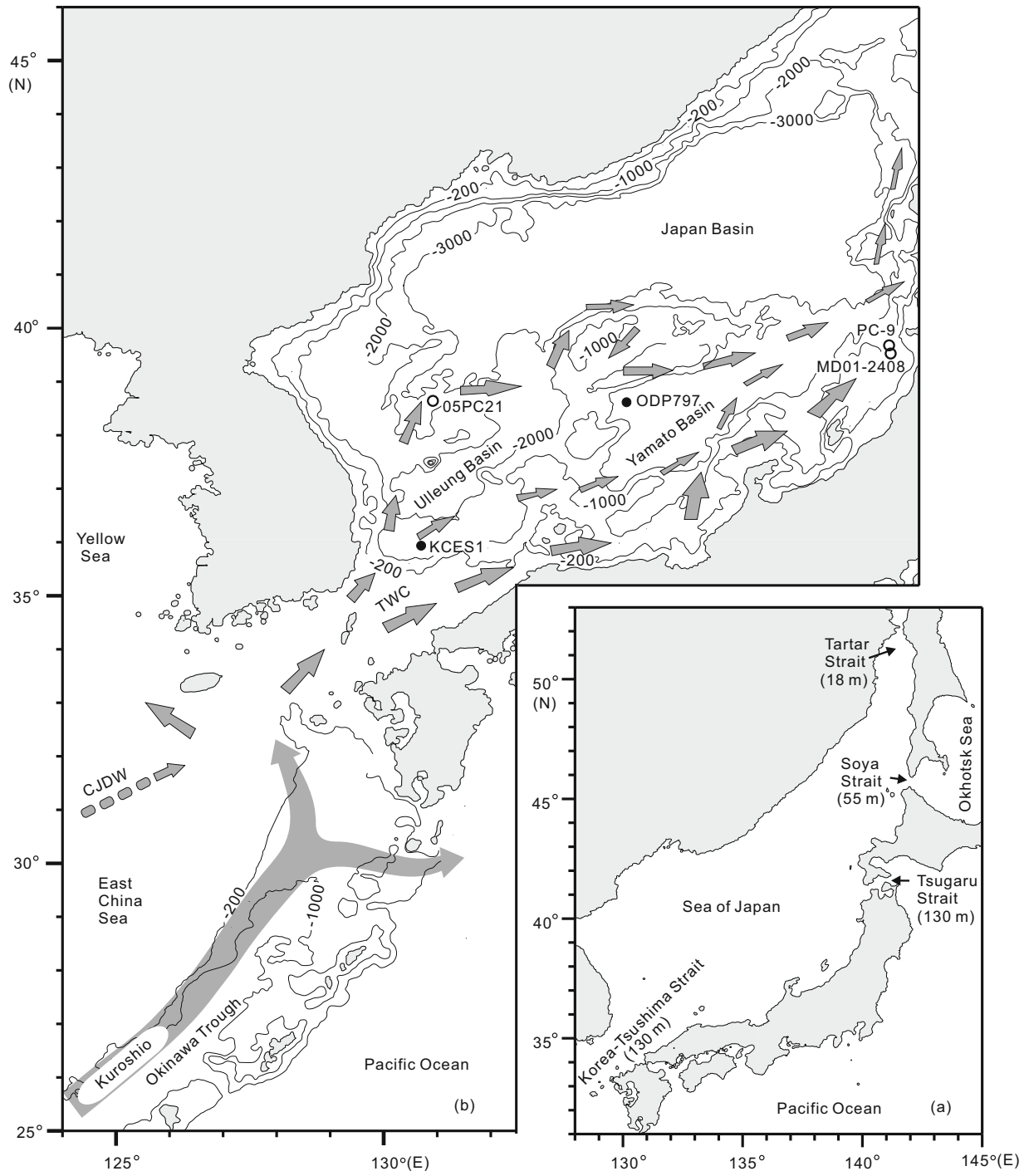

Fig. 1 **a** Location map of the Sea of Japan (JS) with the four main shallow straits connected with the East China Sea, Okhotsk Sea, and the Pacific Ocean; **b** Physiographic sketch and the main warm currents systems in the JS and the East China Sea. The positions of piston core KCES1 and ODP site 797 are shown using black circles, and open circles represent the referred cores in this paper. The simplified bathymetric contours are in meters. *TWC* Tsushima Warm Current, *CJDW* Changjiang diluted water

(D-O) cycles [27, 28]. It is suggested that these dark layers were deposited because of the strong influx of the relatively high nutrient ECSCW and resultant increase in surface productivity [27].

3 Studied cores and age model

Two sedimentary successions were examined in order to construct the $U^{K'}_{37}$-SSTs in the Ulleung and Yamato Basins

of the JS (Fig. 1b). The ODP (Ocean Drilling Program) site 797 (38.62°N, 134.54°E, 2,874 m water depth), which is located 500 km to the northeast of the KTS and slightly south of the northern front of the present TWC, was drilled during the ODP Leg 127 on the northern margin of the Yamato Basin, JS. A continuous late Quaternary sedimentary sequence was recovered and the uppermost 10.37 m was studied in this paper. The deposits of the ODP797 are characterized by distinct alternations of dark and light layers of clay and silty clay with occasional biosiliceous and/or biocalcareous [27].

Piston core KCES1 (35° 56′ 150″ N, 130° 41′ 915″ E, 10.15 m long, and 1,463.8 m water depth) was collected from the southeastern Ulleung Basin, where the sea water was directly influenced by the TWC (Fig. 1b). Similar to the ODP797, the sediments of KCES1 was dominated by clayey silt and silty clay as well as embedded with four tephra layers. Three kinds of sedimentary structures have been identified in the upper part of KCES1 (<730 cm): homogeneous, crudely laminated, and laminated structures based on the data of sediment color (L*), X-ray radiographs, and sediment grain size analyses [29]. Homogeneous and laminated sediments dominated in the upper part; however, the lower part (>730 cm) was so complex in structure that only the upper part of KCES1 was considered in this study.

The chronostratigraphic model of ODP797 and KCES1 was constructed by Tada et al. [27] and Liu et al. [29], respectively, based on AMS ^{14}C age, marker tephra, recognized laminations, and cyclic variation in the diatom abundance in the cores. The studied part of ODP797 and KCES1 represents the paleoceanographic history of the central JS since 170 ka and 48 ka BP, respectively [27, 29].

4 Methods

One hundred and ninety-four samples were taken from the core ODP797 at an interval of 5 cm and a chronostratigraphic resolution of about 0.85 ka, on average. The top 15–20 cm of the core is judged as disturbed because fluidized sediments flowed, which affected only the top two samples [27]. One hundred and eighteen samples were collected at about 6 cm intervals from the KCES1 and represented a mean resolution of 0.41 ka.

Aliquots of 0.5–2 g of the freeze-dried and homogenized sediment were used for alkenone analyses. After adding an internal standard (2-nonadecanone), the samples were extracted by ultrasonication (UP 200H sonic disruptor probe (200 W, amplitude 0.5, pulse 0.5)) using successively less polar mixtures of methanol and methylene chloride (MeOH, MeOH/CH_2Cl_2 1:1, CH_2Cl_2). After each extraction, the samples were centrifuged and the supernatants were combined. The combined extracts were desalted, dried over pre-combusted Na_2SO_4, concentrated under N_2, and finally, absorbed in 25 mL of a 1:1 MeOH/CH_2Cl_2 mixture. The total extracts were purified by solid phase extraction using silica gel cartridges. Solid phase extraction eliminates polar and large molecules. Saponification was performed using 0.1 mol/L KOH in methanol (90/10 CH_3OH/H_2O) at 80 °C for 2 h, and the neutral fraction containing the alkenones was obtained by partitioning into hexane. Abundances of individual compounds were calculated by comparing their peak areas with those of the internal standard (2-nonadecanone). Alkenone contents (per dry weight) are expressed as the total of $C_{37:2}$ and $C_{37:3}$.

The extracts were analyzed by capillary gas chromatography using an HP 5890A gas chromatography equipped with a 50 m × 0.32 mm i.d. HP Ultra 1 fused silica column, split/splitless injection (1:10 split modus), and flame ionization detection. In addition, helium (He) was used as carrier gas. The oven temperature was programmed from 70–250 °C at 20 °C/min and from 250–320 °C at 8 °C/min, and the final temperature was maintained for 45 min. The alkenones were identified by their gas chromatographic retention times by analogy with a synthetic standard. The mean standard error of estimated temperatures for various temperature equations is about 1.1 °C.

The alkenone measurements of KCES1 were conducted at the Department of Geoscience, Bremen University of Germany following the analytical procedures mentioned previously. Alkenone tests of ODP797 were performed at the Laboratory of Marine Chemistry Theory and Technology, Ocean University of China by using of the procedures reported by Xing et al. [30]. The alkenenone data have been reported previously in Xing et al. [31]; however, they are also included in this paper for comparison. $U^{K'}_{37}$-SST values were estimated using the calibrations of Prahl et al. [10] ($U^{K'}_{37} = 0.034T + 0.039$).

One hundred and ninety four samples (ODP 797) and forty five samples (KCES1) were measured for the isotope compositions of total organic carbon ($\delta^{13}C_{org}$) at the Institute of Oceanography, Chinese Academy of Sciences and Ocean University of China, respectively. The samples were first weighted using a cleaned tin cup on a Sartorius 4503 MICRO balance. Capsules that contained measured samples were placed in the Eurovector EA C/N Analyzer and flash burned at 1,030 °C in a quartz combustion tube that contained an atmosphere temporarily enriched with oxygen. Combustion gases were swept through a reduction column (reduction copper) by a stream of inert He gas and passed into a gas chromatography where CO_2 was separated from N_2 and other gases. The gas stream then entered an IsoPrimemass spectrometer where the CO_2 and N_2 gases were analyzed and compared to the standard material for

the carbon and nitrogen isotopes. $\delta^{13}C_{org}$ values are expressed in conventional delta (δ) notation, which is the per mil (‰) deviation from the standard Pee Dee Belemnite (PDB).

5 Results

5.1 Variations of alkenone abundance and $U^{K'}_{37}$ index

Based on the culture experiments with *E. huxleyi* under a growth temperature range of 8–25 °C, Prahl et al. [10] demonstrated that the concentration of the $C_{37:4}$ compound in total alkenones is zero or negligible at or above 15 °C, and that the values of U^{K}_{37} and $U^{K'}_{37}$ are identical in this situation. However, the $C_{37:4}$ alkenone becomes a significant component of alkenones at temperatures <15 °C. The relationship between the $C_{37:4}$ % and temperature is unclear thus far, whereas, the relative abundance of $C_{37:2}$ and $C_{37:3}$ alkenones are linear with the temperature [7]. It has been suggested that there is no relationship between $C_{37:4}$ % and temperature according to the studies performed in the Atlantic, Pacific, and Southern Oceans [32], as well as the Bering Sea [33]. Some published results indicated a strong association of $C_{37:4}$MK with low salinity polar water masses and this relationship was restricted at the high latitude marginal seas thus far [32, 34]. Recent studies on alkenone SST records in the east and west JS indicated that the difference between U^{K}_{37}- and $U^{K'}_{37}$-SSTs were significantly <15 °C, especially during the MIS6 [7, 16]. These results further support that the $C_{37:4}$ % is irrelevant to salinity or temperature in the JS. Therefore, the $U^{K'}_{37}$ index appears to be the better proxy to estimate the SST of the JS.

The variations of C_{37} ($C_{37:2} + C_{37:3}$) alkenone compounds and $U^{K'}_{37}$ values in KCES1 and ODP797 are shown in Fig. 2. In general, both the C_{37} alkenone contents and $U^{K'}_{37}$ values were relatively high during interglacial periods and low during glacial periods. During the penultimate glacial period of 170–130 ka BP (late MIS6), the contents of C_{37} alkenones and $U^{K'}_{37}$ values in the sediments of ODP797 were lower than 2 μg/g and 0.5, respectively. The content of C_{37} alkenones were high during MIS5 (75–130 ka BP) and ranged between 0.15 μg/g (early MIS5) and 20.18 μg/g (MIS5.4). Similar to MIS6, the content of C_{37} alkenones in ODP797 decreased since 75 ka BP and remained very low. During MIS3 and MIS2, the $U^{K'}_{37}$ values varied remarkably with anomalously high values during the LGM (22–19 ka BP), due to the relative low contents of C_{37} alkenone. From 18 ka BP, the $U^{K'}_{37}$ values increased gradually. However, in KCES1 the abundances of C_{37} alkenone increased up to 19.06 μg/g quickly and changed significantly since 15 ka BP (Fig. 2). It particular, indicates that the oceanographic condition of the southern Ulleung Basin is affected by the intrusion of TWC through KTS because of fast sea level rise since 15 ka BP.

5.2 Alkenone-based temperature

The core-top SSTs of KCES1 and ODP797 that was estimated by using the $U^{K'}_{37}$ values is 16.6 °C and 17.5 °C, respectively (Fig. 2). These temperatures are consistent with the annual average SSTs of 16.3 °C and 17.17 °C around the core sites of KCES1 and ODP797, which were calculated statistically using the observed SST data provided by Japan Oceanographic Data Center (JODC, http://jdoss1.jodc.go.jp/cgi-bin/1997/bts). Following the same trend as the variation of $U^{K'}_{37}$ values, the $U^{K'}_{37}$-SSTs are generally relatively high during interglacial periods and low during glacial periods. During MIS6, the $U^{K'}_{37}$-SSTs are generally <10 °C and fluctuate significantly with the lowest temperature (3.8 °C). The alkenone SSTs increased abruptly and vary mainly between 14.2–21.6 °C with an average of 18.3 °C during the MIS5. After MIS4, the $U^{K'}_{37}$-SSTs ranged between 8.8–18.8 °C and display relatively higher levels during MIS3 and MIS1 and with lower ones during MIS4 and late MIS2 (Fig. 2). Anomalously higher $U^{K'}_{37}$-SSTs are presented in the KCES1 and ODP797 during the LGM than those in the Holocene.

6 Discussion

6.1 Unusual alkenone temperatures during LGM

The $U^{K'}_{37}$-SSTs records of the ODP797 and KCES1 revealed that the western JS was warmer during LGM than in the Holocene (Fig. 2). This anomalous trend of high $U^{K'}_{37}$-SSTs is inconsistent with the low glacial temperatures found in the high latitude ice cores [35], the East China Sea [17], the South China Sea [36] and confirmed by previous $U^{K'}_{37}$-SSTs results in the JS [4, 18]. Ishiwatari et al. [18] presented a profile of $U^{K'}_{37}$-SSTs over the past 36 ka, and found that SSTs during the LGM were much higher than previously assumed. The $U^{K'}_{37}$-SSTs records from core MD01-2408 [4] and core 05PC21 [7] also show the same unusually high temperatures during the MIS2 and MIS3.

It seems that there is no dispute about the unusually high alkenone temperatures during the LGM in the JS. However, the reason for the $U^{K'}_{37}$-SSTs' anomaly remains controversial. Ishiwatari et al. [18] suggested that during the LGM, the water column of the JS became stratified as sea level dropped. Therefore, the high mean annual SSTs may have occurred under heavily stratified surface seawater where

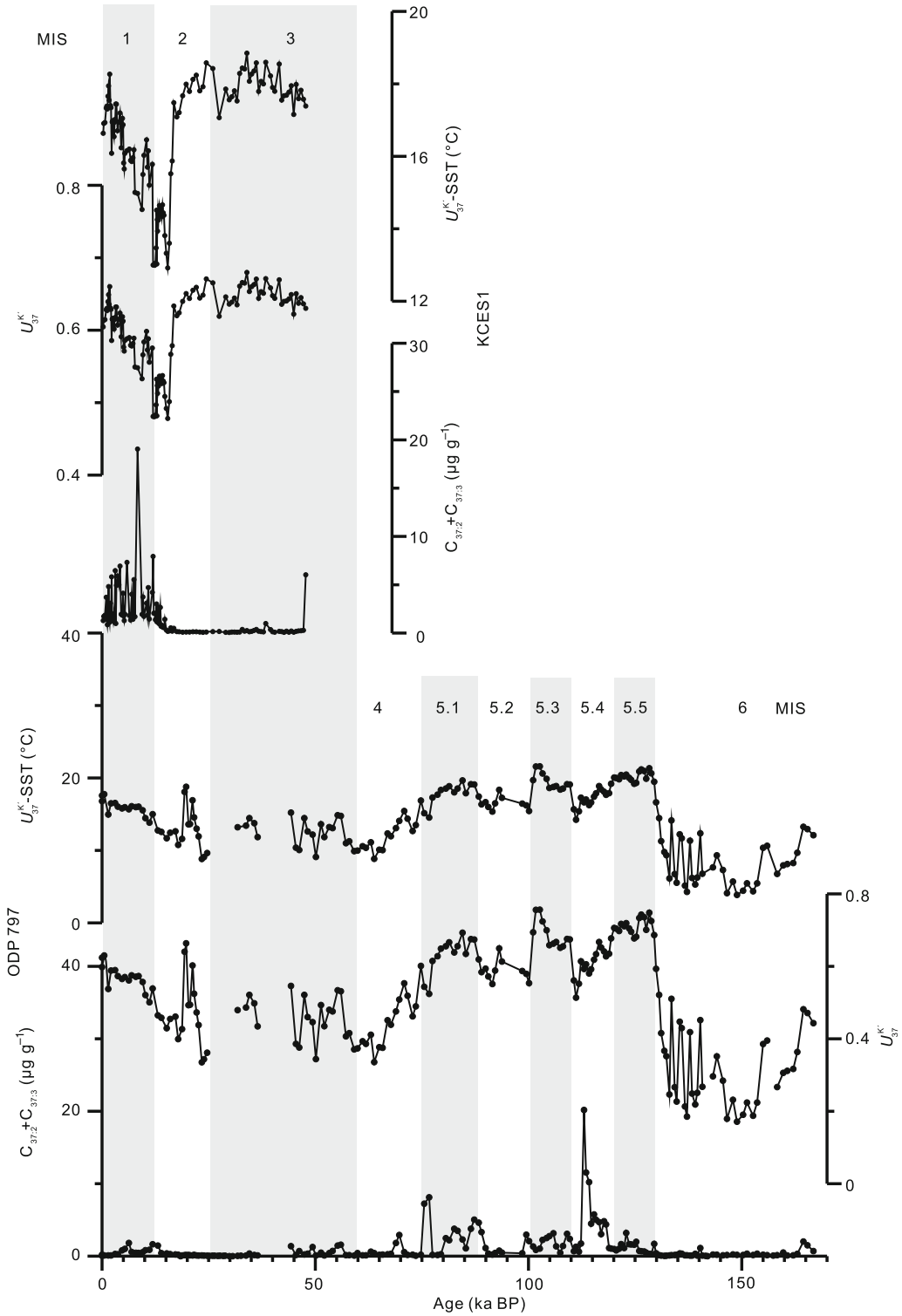

Fig. 2 The contents of C_{37} alkenone ($C_{37:2}$+$C_{37:3}$), the $U^{K'}_{37}$ and the $U^{K'}_{37}$-SSTs (calculated by the equation in [10]) versus age in ODP797 and core KCES1. The gray bars indicate marine isotope stages (MIS)

thermal energy due to solar radiation was trapped in shallow waters. However, this mechanism has not been supported by other additional studies. Micropaleontological studies revealed cold surface water conditions in the JS during the LGM [37–39]. Other likely explanations for the LGM anomaly could be that much lower salinity resulted

in higher SST [16]. However, Lee et al. [7] reported low salinity during MIS6 in the JS but no unusually high $U^{K'}_{37}$-SSTs was confirmed, and therefore, suggested that the salinity anomaly might not be the dominant reason for the LGM unusually high $U^{K'}_{37}$-SSTs recorded in the JS. Additional studies are still needed to evaluate the reason of the anomalous high alkenone SSTs during the LGM.

The $\delta^{13}C_{org}$ values of sedimentary organic matter in deep-sea sediments are used to estimate the relative contributions of terrigenous organic matter and as a proxy for the degree of dissolved oxygen concentration in the JS [40, 41]. When the relative proportion of terrigenous organic matters increases, which may be induced by the virtual increases of terrigenous supply due to the sea level drop or the decreases of marine primary production, the $\delta^{13}C_{org}$ values will be more negative and vice versa. The $\delta^{13}C_{org}$ values in the JS seem to vary consistently with late Pleistocene paleoclimatic change, although it is not systematically correlated with glacial-interglacial stages [40]. Figure 3 presents comparative records of the $U^{K'}_{37}$-SSTs and $\delta^{13}C_{org}$ data of the ODP797 and KCES1. Generally, the $\delta^{13}C_{org}$ records of ODP797 are higher during the interglacial than during the glacial and show similar trends as the $U^{K'}_{37}$-SSTs records with the exclusion of during the LGM, MIS4, and late MIS5 (Fig. 3b). Since the resolution is relatively low and lacks reliable evidence, the controlling forces resulted in the difference between $\delta^{13}C_{org}$ and $U^{K'}_{37}$-SSTs records during MIS4 and late MIS5 in ODP 797 are remained unclear so far. During the LGM, the $\delta^{13}C_{org}$ of ODP797 and KCES1 represent most negative values (Fig. 3b and e), which implies the enhanced contribution of terrestrial organic detritus. Minoura et al. [41] first reported that a higher terrestrial input period occurred in the LGM as revealed by the much lower bulk organic carbon isotope $\delta^{13}C$ records from the Yamato Basin. Increased Aeolian contribution of terrigenous particles in the form of Aeolian dust supplied from inland China was reported in the JS during the LGM [42]. The low mass accumulation rate (MAR) of total organic carbon (TOC) and carbonate content ($CaCO_3$) [43] and the negative shift of the $\delta^{13}C_{org}$ value (Fig. 3e) from the KCES1 indicate low productivity sea surface prevailed during the period 48–18 ka BP due to limited water exchange and relatively higher terrestrial material supply.

Higher values of the bulk sediment flux (Fig. 3a), the percentage of *Parlia Sulcata* (*P. Sulcata*) (Fig. 3c), and the content and MAR of terrestrial organic matter (TOM) (Fig. 3d) were recorded in LGM and MIS6 [27, 31]. As inferred by Tada et al. [27] and Xing et al. [31], the higher percentage of *P. Sulcata* indicates an increasing input of the lower salinity water mass; meanwhile, the higher TOM contents and MAR suggest a larger proportion of terrigenous material discharged into the JS. Thus, these multi-proxies records could indicate an enhanced influence of low salinity water mass intrusion and increased terrestrial inputs into the JS in the LGM and MIS6. It is notable that the enhanced influence of low salinity water and increased terrestrial input during the glacial were previously confirmed. Oba et al. [19] suggested that the estuary of the Yellow River shifted to the east side of Cheju Island during the last glacial period and thus, the cold low salinity water intruded into the JS. Recently, paleo-productivity records based on biomarkers showed a quite low coccolith production during the LGM in the JS because of the influence of lower salinity water mass [31]. In the glacial, the intrusion of the TWC was restricted due to lower sea level and shallower KTS. While low salinity ECSCW, which was derived mainly from the Changjiang and the Yellow River, could invade the JS from the KTS. Moreover, the other alkenone-based temperature reconstruction shows that the climate was cold and moist in the JS during the last glacial period [7]. Both may reduce the surface salinity of the JS.

The effects of the intrusion of lower salinity water and the high terrestrial input occurred in the LGM and MIS6; however, the comparison in Fig. 3 shows a stronger influence occurred in the LGM than in the early MIS6 for core ODP797 (Fig. 3c, d). We attributed this might to the lower salinity in the LGM than in the MIS6 for the JS. As indicated by Fujine et al. [4, 16], the anomalously high $U^{K'}_{37}$-SSTs in the LGM for core MD01-2408 were always accompanied by high levels of $C_{34:2}$EE. Fujine et al. [4, 16] noted that the extremely low salinity level could have an ecological or physiological influence on both the unsaturation and carbon chain length of alkenones and alkenoates (e.g. lower salinity prefer a high portion of $C_{34:2}$EE and anomaly high $U^{K'}_{37}$-SSTs [32]). Since no $C_{34:2}$EE was detected from core ODP797, the biomarker records reveal the strongest influences of low salinity water intrusion and terrestrial inputs in the LGM (Fig. 3). The extremely low salinity condition might affect and restrict the alkenone producer species, resulted in anomalously high $U^{K'}_{37}$-SSTs in the LGM. Although the influence of low salinity water and terrestrial input was somewhat strong during MIS6, the alkenone producer might have lower restriction. However, the explanations for the alkenone-based SSTs difference between the LGM and MIS6 still in arguing. Higher resolution and multi-proxies study are needed in the future.

6.2 Variation in $U^{K'}_{37}$-temperature during the last 170 ka and its implications

The $U^{K'}_{37}$-SSTs records from the MD01-2408 [4], 05PC21 [7], and ODP797 cores were adopted to trace the SST history of the JS for the last 170 ka (Fig. 4). All three SST

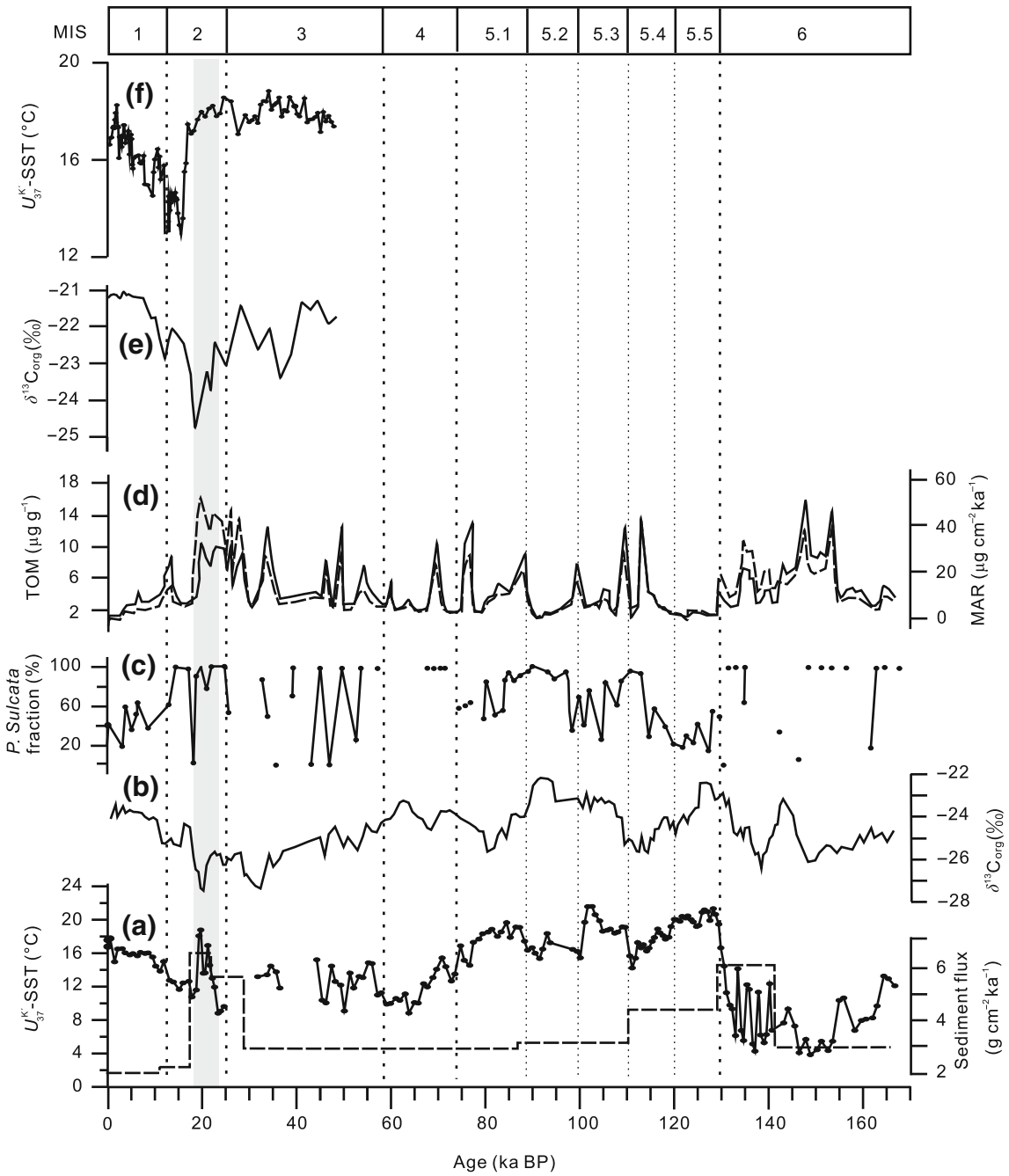

Fig. 3 **a** $U^{K'}_{37}$-SSTs (solid line) and bulk sediment influx (dashed line, [31]) for ODP797; **b** $\delta^{13}C_{org}$ record for ODP 797; **c** *P. Sulcata* fraction for ODP797 [27]; **d** content (solid line) and mass accumulation rates (dashed lines) of the terrestrial organic matter (TOM) for ODP797 [31]; **e** $\delta^{13}C_{org}$ record for KCES1; f $U^{K'}_{37}$-SSTs for core KCES1. MIS is labeled on the top panels. The anomalously high $U^{K'}_{37}$-SSTs during the LGM are highlighted by gray bar

records show a similar pattern on the glacial-interglacial to orbital timescale (>10^4 a) since MIS6, considering the diverse temporal resolution. Perceptible differences can be observed in the three records on sub-orbital/millennial (<10^4 a) timescale. For example, records from core ODP797 reveal a notable SST variation during MIS5, while in MIS2 and MIS3 the resolution of $U^{K'}_{37}$-SSTs records is very low. Because cores MD01-2408 and 05PC21 present good resolution for these periods, we make a comparative analysis for all three $U^{K'}_{37}$-SSTs records in this study to reconstruct the history of SST variation in the JS.

Figure 4 offers the combined three $U^{K'}_{37}$-SSTs records of the JS with a comparison of the Northern Hemisphere

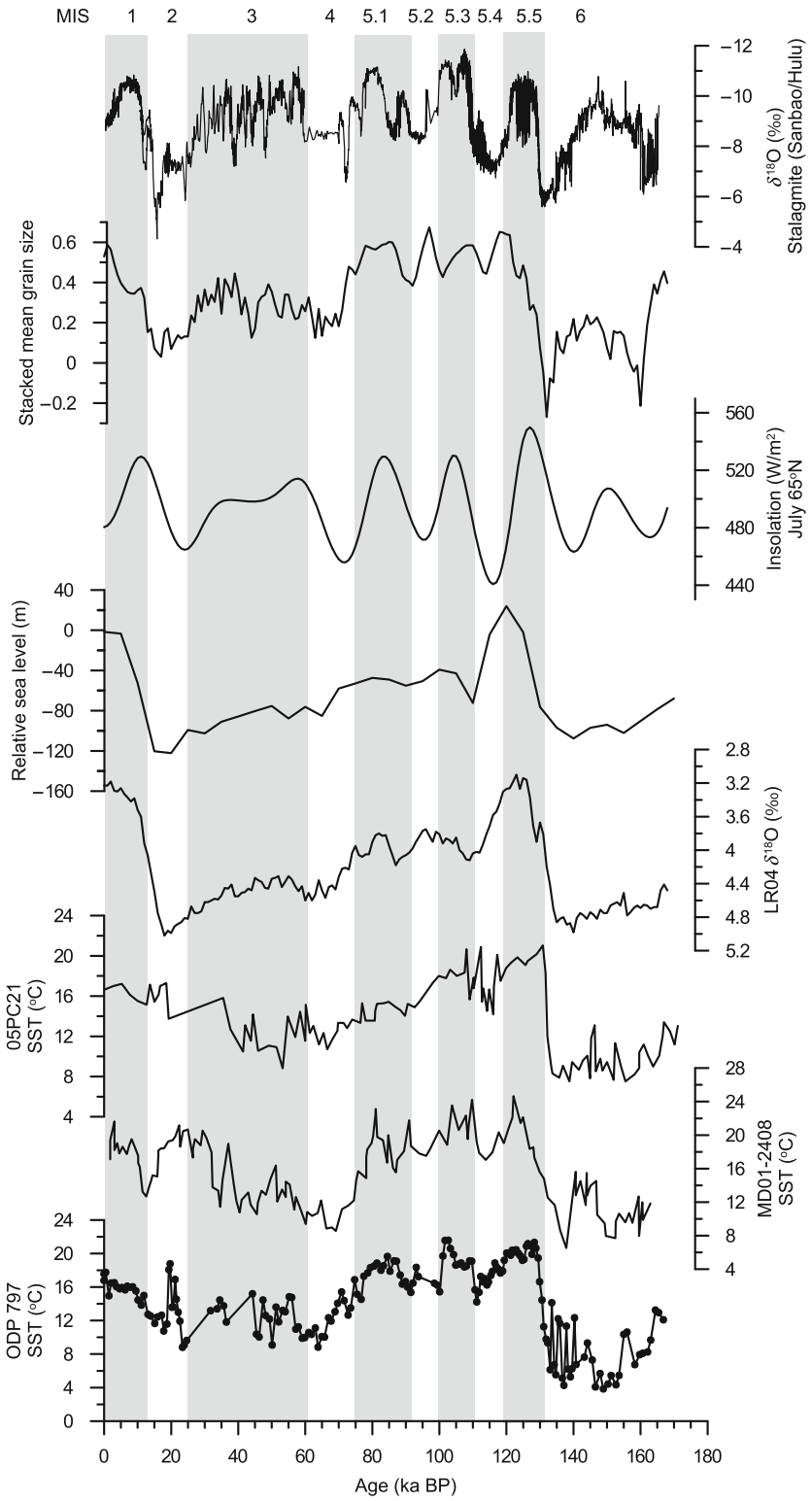

Fig. 4 Variation in $U^{K'}_{37}$-SSTs of ODP797 and comparison with $U^{K'}_{37}$-SSTs of MD01-2908 [4], $U^{K'}_{37}$-SSTs of 05PC21 [7], benthic stacked δ^{18}O [48], relative sea level curve [47], insolation in July at 65°N [44], stacked mean grain size of the loess-paleosol sequence [45] and Sanbao/Hulu δ^{18}O records [46]

summer insolation on July 21 at 65°N [44], the Asian monsoon [45, 46], the global relative sea level curve, [47] and the benthic foraminiferal δ^{18}O records for the marine sediments [48]. The result reveals that over a glacial-interglacial timescale, the $U^{K'}_{37}$-SSTs records of JS correlated with the benthic foraminiferal δ^{18}O records [48],

which is considered an indicator of the growth and decay of the northern Hemisphere ice sheets. Furthermore, the combined $U^{K'}_{37}$-SST records broadly follow the orbitally induced Northern Hemisphere summer insolation. This indicates that the SST of the JS may be generally controlled by the solar insolation and the related sea ice growth and decay in the glacial-interglacial cycle. In glacial cycles, the ice-sheet of the north Hemisphere expanded and the global sea level retained in a quite low level. It was believed that the sea level of the JS dropped to approximately −130 m below present during the LGM and MIS6 (Fig. 4). Since the sill depths in the KTS is <130 m [18], the shallower water depth at the KTS prevented the warm TWC from entering the JS [38], which resulted in a decreased SST in the JS during MIS6. In addition, the expansion of ice-sheet would lead to strengthened cold conditions globally that may partly be responsible for the decreased SST in the glacial period of the JS considering that large temperature contrasts existed between the glacial-interglacial period.

On a sub-orbital/millennial scale, the $U^{K'}_{37}$-SSTs records closely correspond to the variations of East Asian Winter Monsoon (EAWM) in the last glacial period. For example, during MIS3 and MIS4, each reduced SST stage corresponds to an enhanced EAWM period indicated by the stacked mean grain size of the loess sequence from the Chinese Loess Plateau (Fig. 4) [45]. The winter monsoon is characterized by cold air masses blowing from the Siberian high to the surrounding lows. When the winter monsoon intensified, the colder air and strengthened wind from the North not only could contribute to the JS surface cooling [7], but could also induce an increase of sea-ice in JS. Modern observation shows that sea-ice expansion in the modern Russian coast is controlled primarily by the strength and direction of wind over the sea [49]. Since the predominant wind direction of the modern winter monsoon is northwest in the JS, which is nearly normal to the Russian coast, a stronger winter monsoon is expected to result in an enlarged sea-ice expansion and further reduction of SST in the JS [6].

In the interglacial cycles, the $U^{K'}_{37}$-SSTs records varied in synchrony with the East Asian Summer Monsoon (EASM) (Fig. 4). Higher $U^{K'}_{37}$-SSTs correspond with the enhanced EASM in MIS5.5, MIS5.3, and MIS5.1. When the EASM is depressed in MIS5.2 and MIS5.4, lower $U^{K'}_{37}$-SSTs were recorded in the ODP797 (Fig. 4). Though the relative sea level varied in the interglacial period, the maximum global sea level change due to changes in the ice-volume is considered to be <60 m during the stage of MIS5, since the straits were most likely wide enough to allow the inflow and outflow in the JS. Therefore, the changes of inflow did not play a significant role in JS alkenone temperature changes during the MIS5 [7]. Close correlations between the $U^{K'}_{37}$-SSTs and the EASM records indicate that the sea surface temperatures in the eastern JS may be related to the changes in the EASM activity during the interglacial period [4]. According to Lee et al. [7], the intensity of the EASM could affect the migration of the sub polar front. In the interglacial period, solar irradiation increased and resulted in an enhanced EASM and subtropical high, which moved the sub polar front northward and developed a higher SST in the JS. Moreover, the intensity of EASM may influence the inflow of the TWC. An increased EASM induced an enlarged inflow of Changjiang diluted water into the East China Sea, which decreased the density of the East China Sea water mass, and subsequently the pressure gradient between the entrance of the KTS and the exit of the Tsugaru Strait was enlarged [4]. This favored the strengthening of the warm TWC into the JS, and induced an increased SST in the interglacial period.

Overall, these results indicate that on a sub-orbital/millennial timescale the SST of the JS may be related to the intensity of the EAM, as an enhanced EASM or a depressed EAWM may result in higher interglacial SST.

7 Conclusions

This study presents the alkenone records from the western and central area of the JS for a period of 170 ka BP, leading to the following conclusions.

(1) The $U^{K'}_{37}$ records of the ODP 797 and KCES1 revealed that SSTs in the glacial period was lower than that in the interglacial period, except in the MIS2 during which the SST was higher than in the Holocene. During the MIS5, the temperature fluctuated from 20.1 °C to 17 °C to 19.6 °C at MIS5.5, MIS5.4, and MIS5.3, respectively. At MIS5.2, the SSTs decreased to 16.5 °C and increased to 17.8 °C again at MIS5.1.

(2) On a glacial-interglacial timescale, the $U^{K'}_{37}$-SSTs records of ODP 797 in the JS correlated with the benthic foraminiferal $\delta^{18}O$ record and summer insolation, which suggests that the dominant control of solar insolation and the related sea ice growth and decay in the glacial-interglacial cycle on the SST in the JS since the last 170 ka BP.

(3) On a sub-orbital/millennial timescale, during the last glacial period (MIS3 and MIS4), each reduced SST stage corresponds to an enhanced EAWM period. These findings suggest that a stronger winter monsoon is expected to result in an enlarged sea-ice expansion and further reduction in the SST of the JS. In contrast, during the interglacial period (MIS5), the $U^{K'}_{37}$-SSTs records varied in synchrony with the EASM, suggesting the dominant control of enhanced EASM on the increased SST in the JS.

Acknowledgments This work was supported by the National Natural Science Foundation of China (41076038, 40710069004, 40606016 and 41006036), and the Project of Global Change and Air-Sea Interaction.

References

1. Ikeda M, Suzuki F, Oba T (1999) A box model of glacial-interglacial variability in the Japan Sea. J Oceanogr 55:483–492
2. Yoon JH, Kawamura H (2002) The formation and circulation of the intermediate water in the Japan Sea. J Oceanogr 58:197–211
3. Chang KI, Teague WJ, Lyu SJ et al (2004) Circulation and currents in the southwestern East/Japan Sea: overview and review. Prog Oceanogr 61:105–156
4. Fujine K, Tada R, Yamamoto M (2009) Paleotemperature response to monsoon activity in the Japan Sea during the last 160 kyr. Palaeogeogr Palaeoclimatol Paleoecol 280:350–360
5. Lee KE (2007) Surface water changes recorded in Late Quaternary marine sediments of the Ulleung Basin, East Sea (Japan Sea). Palaeogeogr Palaeoclimatol Paleoecol 247:18–31
6. Ikehara K, Itaki T (2007) Millennial-scale fluctuations in seasonal sea-ice and deep-water formation in the Japan Sea during the late Quaternary. Palaeogeogr Palaeoclimatol Paleoecol 247:131–143
7. Lee KE, Bahk JJ, Choi J (2008) Alkenone temperature estimates for the East Sea during the last 190,000 years. Org Geochem 39:741–753
8. Volkman JK, Barrett SM, Blackburn SI et al (1995) Alkenones in Gephyrocapsa oceanica: implications for studies of paleoclimate. Geochim Cosmochim Acta 59:513–520
9. Brassell SC, Eglinton G, Marlowe IT et al (1986) Molecular stratigraphy: a new tool for climatic assessment. Nature 320:129–133
10. Prahl FG, Muehlhausen LA, Zahnle DL (1988) Further evaluation of long-chain alkenones as indicators of paleoceanographic conditions. Geochim Cosmochim Acta 52:2303–2310
11. Eglinton T, Conte M, Eglinton G et al (2000) Alkenone biomarkers gain recognition as molecular paleoceanographic proxies. Eos 81:253–260
12. Freeman KH, Wakeham SG (1992) Variations in the distributions and isotopic compositions of alkenones in Black Sea particles and sediments. Org Geochem 19:277–285
13. Sikes EL, Farrington JW, Keigwin LD (1991) Use of the alkenone unsaturation ratio $U^{K'}_{37}$ to determine past sea surface temperatures: core-top SST calibrations and methodology considerations. Earth Planet Sci Lett 104:36–47
14. Sikes EL, Volkman JK, Robertson LG et al (1997) Alkenones and alkenes in surface waters and sediments of the Southern Ocean: implications for paleotemperature estimation in polar regions. Geochim Cosmochim Acta 61:1495–1505
15. Weaver PPE, Chapman MR, Eglinton G et al (1999) Combined coccolith, foraminiferal, and biomarker reconstruction of paleoceanographic conditions over the past 120 kyr in the northern North Atlantic (59°N, 23°W). Paleoceanography 14:336–349
16. Fujine K, Yamamoto M, Tada R et al (2006) A salinity related occurrence of a novel alkenone and alkenoate in late Pleistocene sediments from the Japan Sea. Org Geochem 37:1074–1084
17. Ijiri A, Wang LJ, Oba T et al (2005) Paleoenvironmental changes in the northern area of the East China Sea during the past 42,000 years. Palaeogeogr Palaeoclimatol Paleoecol 219:239–261
18. Ishiwatari R, Houtatsu M, Okada H (2001) Alkenone–sea surface temperatures in the Japan Sea over the past 36 kyr: warm temperatures at the last glacial maximum. Org Geochem 32:57–67
19. Oba T, Kato M, Kitazato H et al (1991) Paleoenvironmental changes in the Japan Sea during the last 85,000 years. Paleoceanography 6:499–518
20. Matsui H, Tada R, Oba T (1998) Low-salinity isolation event in the Japan Sea in response to eustatic sea-level drop during LGM: Reconstruction based on salinity-balance model. Quat Res 37:221–233 (in Japanese)
21. Kim K, Kim KR, Kim YG et al (1996) New findings from CREAMS observations: water masses and eddies in the East Sea. J Korean Soc Oceanogr 31:155–163
22. Gamo T (1999) Global warming may have slowed down the deep conveyer belt of a marginal sea of the northwestern Pacific: Japan Sea. Geophys Res Lett 26:3137–3140
23. Yokoyama Y, Kido Y, Tada R et al (2007) Japan Sea oxygen isotope stratigraphy and global sea-level changes for the last 50,000 years recorded in sediment cores from the Oki Ridge. Palaeogeogr Palaeoclimatol Paleoecol 247:5–17
24. Kumamoto Y, Yoneda M, Shibata Y et al (1998) Direct observation of the rapid turnover of the Japan Sea bottom water by means of AMS radiocarbon measurement. Geophys Res Lett 25:651–654
25. Isobe A (1999) On the origin of the Tsushima warm current and it seasonality. Cont Shelf Res 19:117–133
26. Bahk JJ, Chough SK, Han SJ (2000) Origins and paleoceanographic significance of laminated muds from the Ulleung Basin, East Sea (Sea of Japan). Mar Geol 162:459–477
27. Tada R, Irino T, Koizumi I (1999) Land-ocean linkages over orbital and millennial timescales recorded in late Quaternary sediments of the Japan Sea. Paleoceanography 14:236–247
28. Yao ZQ, Liu YG, Shi XF et al (2012) Paleoenvironmental changes in the East/Japan Sea during the last 48 ka: indications from high-resolution X-ray fluorescence core scanning. J Quat Sci 27:932–940
29. Liu YG, Sha LB, Shi XF et al (2010) Depositional environment in the southern Ulleung Basin, East Sea (Sea of Japan), during the last 48,000 years. Acta Oceanol Sin 29:52–64
30. Xing L, Zhao MX, Zhang HL et al (2008) Biomarker reconstruction of phytoplankton productivity and community structure changes in the middle Okinawa Trough during the last 15 ka. Chin Sci Bull 53:2552–2559
31. Xing L, Zhang RP, Liu YG et al (2011) Biomarker records of phytoplankton productivity and community structure changes in the Japan Sea over the last 166 kyr. Quat Sci Rev 30:2666–2675
32. Sikes EL, Sicre MA (2002) Relationship of the tetra-unsaturated C_{37} alkenone to salinity and temperature: implications for paleoproxy applications. Geochem Geophys Geosyst. doi:10.1029/2002GC000345
33. Harada N, Shin KH, Murata A et al (2003) Characteristics of alkenones synthesized by a bloom of *Emiliania huxleyi* in the Bering Sea. Geochim Cosmochim Acta 67:1507–1519
34. Bendle J, Rosell-Mele A, Ziveri P (2005) Variability of unusual distribution of alkenones in the surface waters of the Nordic seas. Paleoceanography 20:1830. doi:10.1029/2004PA001025
35. Petit JR, Jouzel J, Raynaud D et al (1999) Climate and atmospheric history of the past 420,000 years from the Vostok ice core, Antarctica. Nature 399:429–436
36. Zhao MX, Huang CY, Wang CC et al (2006) A millennial-scale $U^{K'}_{37}$ sea-surface temperature record from the South China Sea (8°N) over the last 150 kyr: monsoon and sea-level influence. Palaeogeogr Palaeoclimatol Paleoecol 236:39–55
37. Nakagawa T, Kitagawa H, Yasuda Y et al (2003) Yangtze River Civilization Program Members. Asynchronous climate changes in the north Atlantic and Japan during the last termination. Science 299:688–691
38. Itaki T, Komatsu N, Motoyama I (2007) Orbital- and millennial-scale changes of radiolarian assemblages during the last 220 kyrs in the Japan Sea. Palaeogeogr Palaeoclimatol Paleoecol 247:115–130

39. Koizumi I, Tada R, Narita H et al (2006) Paleoceanographic history around the Tsugaru Strait between the Japan Sea and the Northwest Pacific Ocean since 30 cal kyr BP. Palaeogeogr Palaeoclimatol Paleoecol 232:36–52
40. Khim BK, Ikehara K, Bahk JJ, Irino T (2008) Increased negative anomalies of sedimentary organic matter δ^{13}C and δ^{15}N values in the East Sea (Sea of Japan) during the full glaciation of the late Quaternary. Quat Int 7:25–35
41. Minoura K, Hoshino K, Nakamura T et al (1997) Late Pleistocene-Holocene paleoproductivity circulation in the Japan Sea: sea-level control on δ^{13}C and δ^{15}N records of sediment organic material. Palaeogeogr Palaeoclimatol Paleoecol 135:41–50
42. Irino T, Tada R (2002) High-resolution reconstruction of variation in Aeolian dust (Kosa) deposition at ODP site 797, the Japan Sea, during the last 200 ka. Global Planet Change 35:143–156
43. Zou JJ, Shi XF, Liu YG et al (2012) Reconstruction of environmental changes using a multi-proxy approach in the Ulleung Basin (Sea of Japan) over the last 48 ka. J Quat Sci 27:891–900
44. Berger AL (1978) Long-term variations of caloric insolation resulting from the Earth's orbital elements. Quat Res 9:139–167
45. Sun YB, Clemens SC, An ZS et al (2006) Astronomical timescale and palaeoclimatic implication of stacked 3.6 Myr monsoon records from the Chinese Loess Plateau. Quat Sci Rev 25:33–48
46. Wang YJ, Cheng H, Edwards RL et al (2008) Millennial- and orbital-scale changes in the East Asian monsoon over the past 224,000 years. Nature 451:1090–1093
47. Miller KG, Kominz MA, Browning JV et al (2005) The Phanerozoic record of global sea level change. Science 310:1293–1298
48. Lisiecki LE, Raymo ME (2005) A Pliocene-Pleistocene stack of 57 globally distributed benthic δ^{18}O records. Paleoceanography. doi:10.1029/2004PA001071
49. Shimada T, Kawamura H (2006) Satellite observations of sea-surface temperature and sea-surface wind coupling in the Japan Sea. J Geophys Res. doi:10.1029/2005JC003345